Supplementary Information

Conjugated Metallorganic Macrocycles: Opportunities for Coordination-Driven Planarization of Bidentate, Pyridine-Based Ligands

Danielle C. Hamm,[†] Lindsey A. Braun,[†] Alex N. Burazin,[†] Amanda M. Gauthier,[†] Kendra O. Ness,[†] Casey E. Biebel,[†] Jon S. Sauer,[†] Robin S. Tanke,[†] Bruce C. Noll,[§] Eric Bosch[‡] and Nathan P. Bowling*[†]

[†]*Department of Chemistry, University of Wisconsin-Stevens Point, 2001 Fourth Avenue, Stevens Point, WI, 54481*
[‡]*Department of Chemistry, Missouri State University, 901 S. National Ave., Springfield, MO, 65897*
[§]*Bruker AXS Inc., 5465 East Cheryl Parkway, Madison, WI, 53711*

Table of Contents

^{1}H and ^{13}C Spectra of Compounds	S2-S13
NMR titration of Ligand **1** and Ligand **2** With AgOTf and $PdCl_2(PhCN)_2$	S14-S17
Absorption and Fluorescence Spectra For **1**, **2** and Complexes	S18-S19
Crystal Data for **1**, **2** and Complexes	S20-S26

^{1}H and ^{13}C NMR spectra

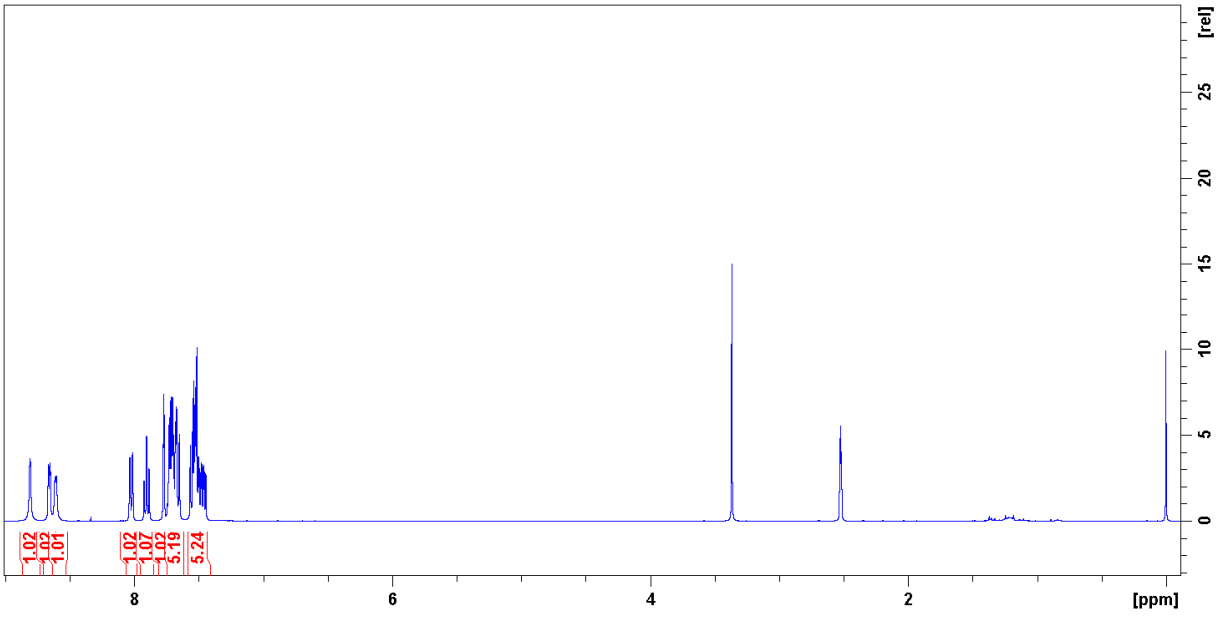

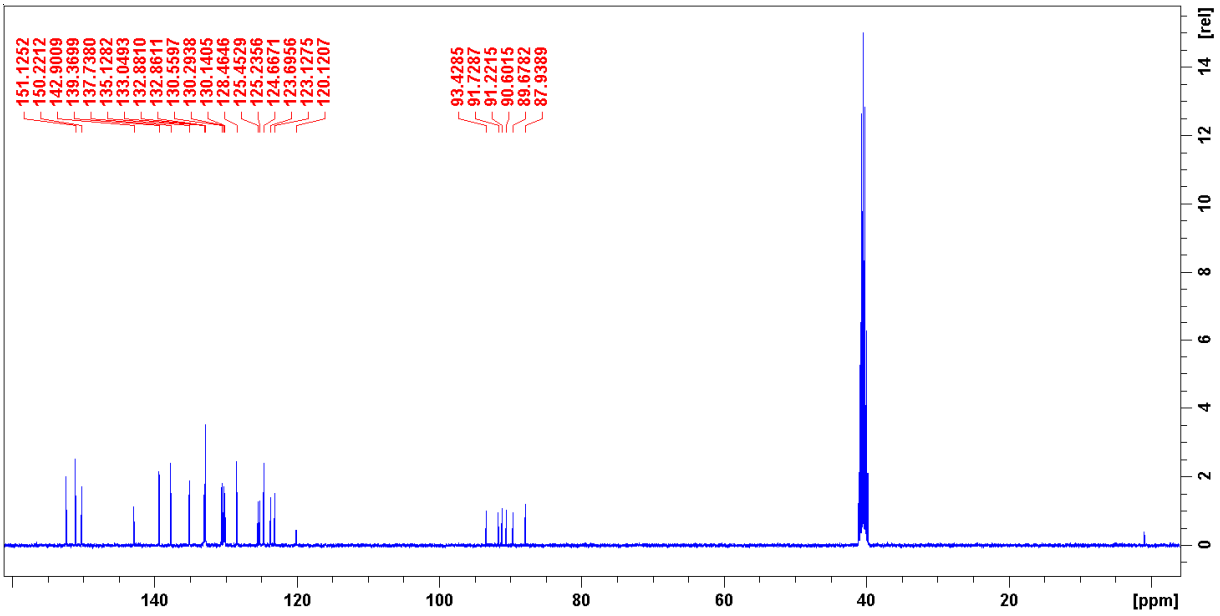

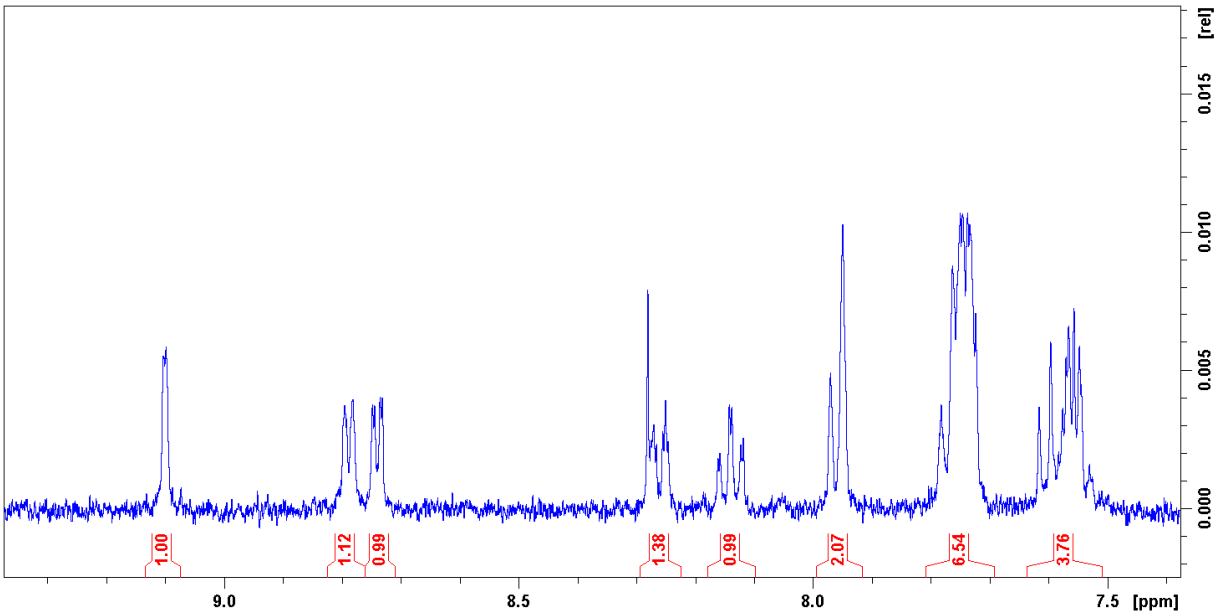
[rel]
0.015
0.010
0.005
0.000
1.00
1.12
0.99
1.38
0.99
2.07
6.54
3.76
9.0
8.5
8.0
7.5 [ppm]

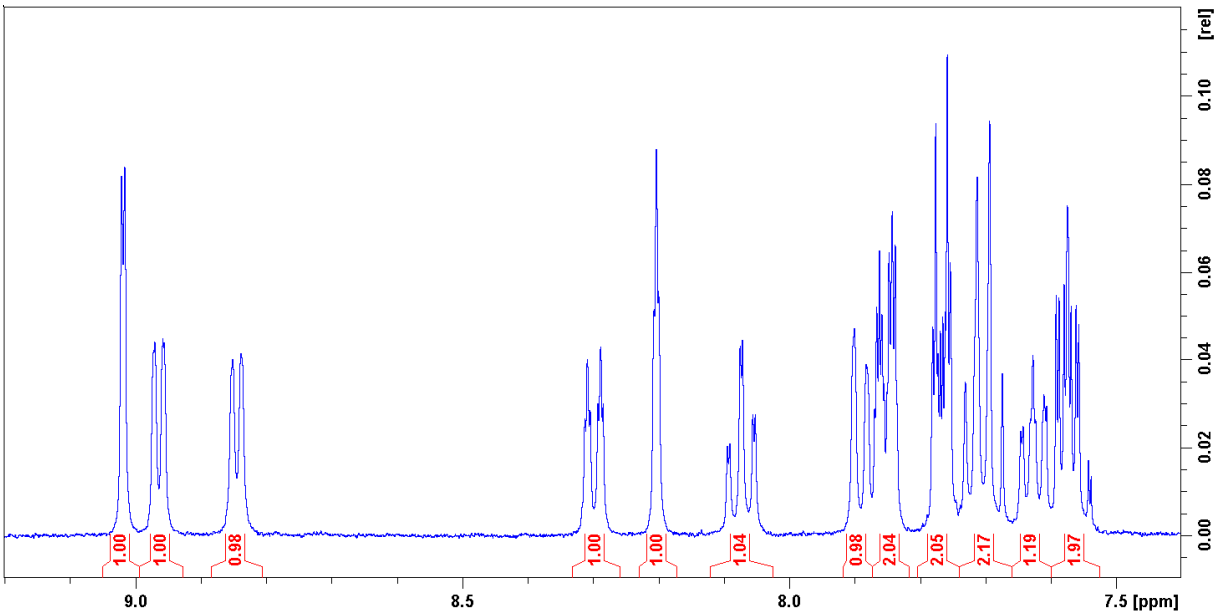
[rel]
0.10
0.08
0.06
0.04
0.02
0.00
1.00
1.00
0.98
1.00
1.00
1.04
0.98
2.04
2.05
2.17
1.19
1.97
9.0
8.5
8.0
7.5 [ppm]

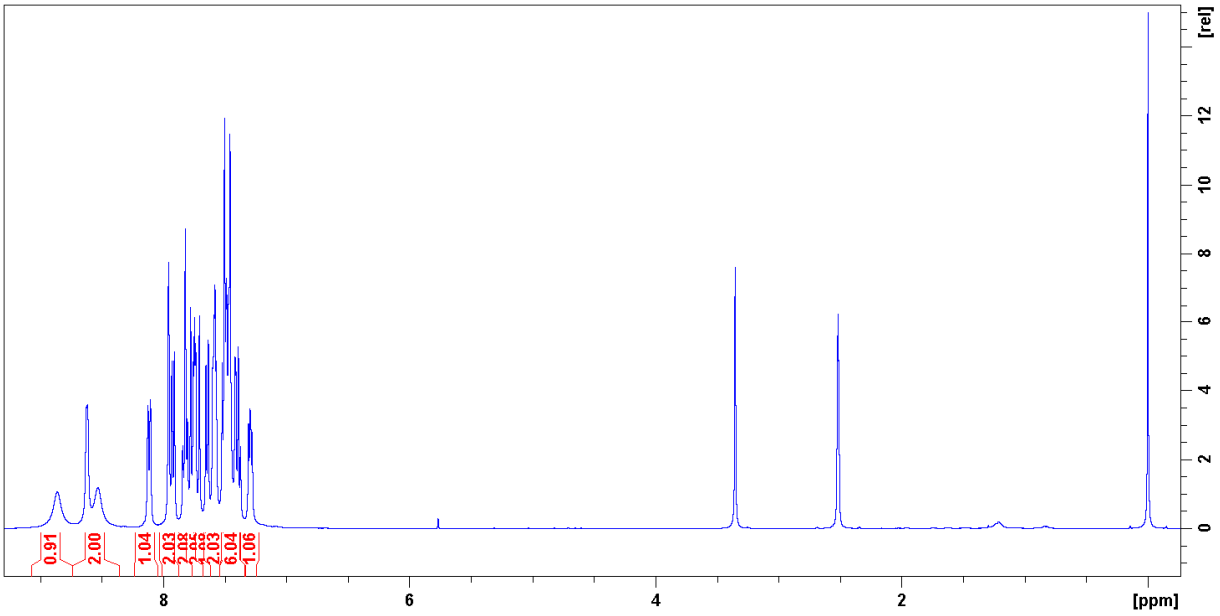

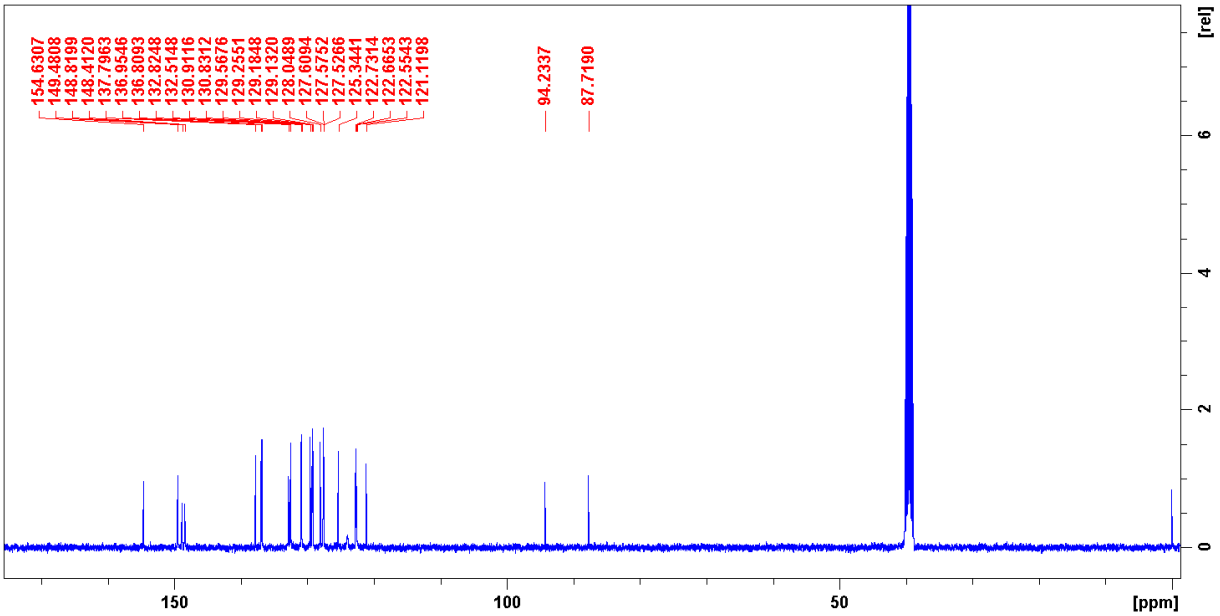

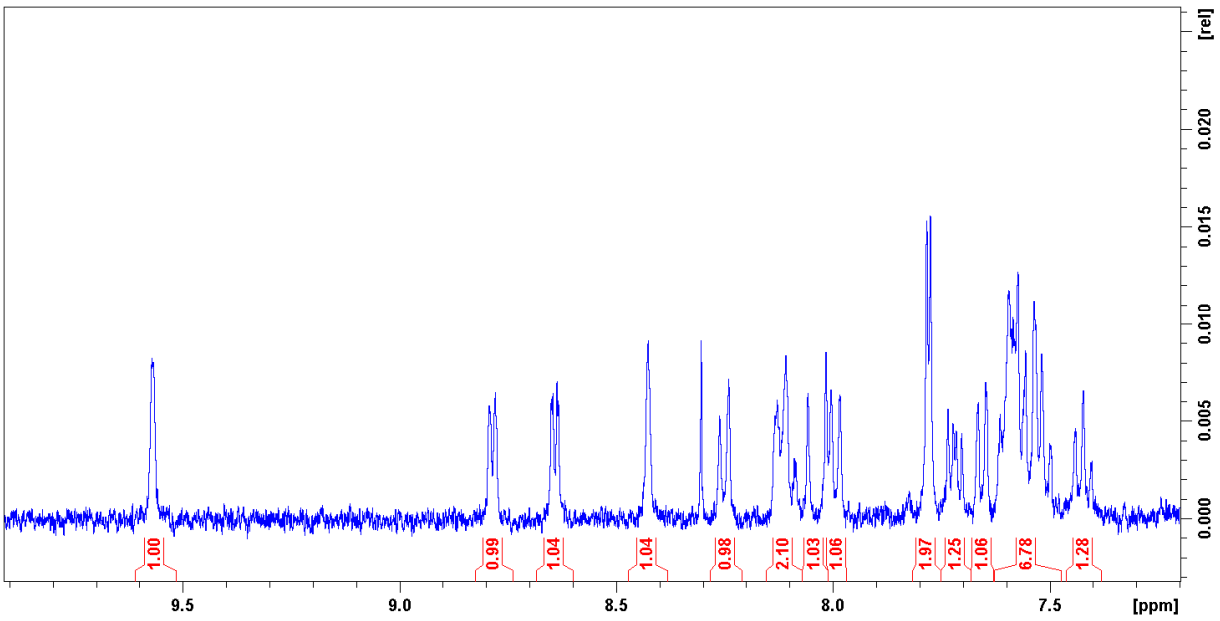

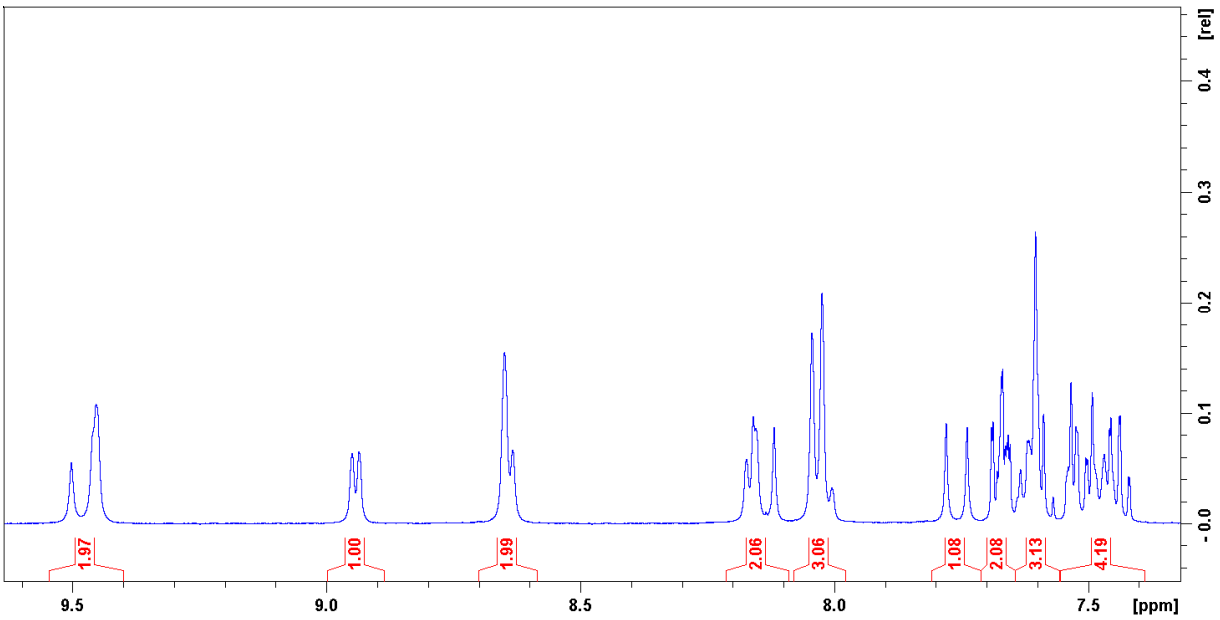

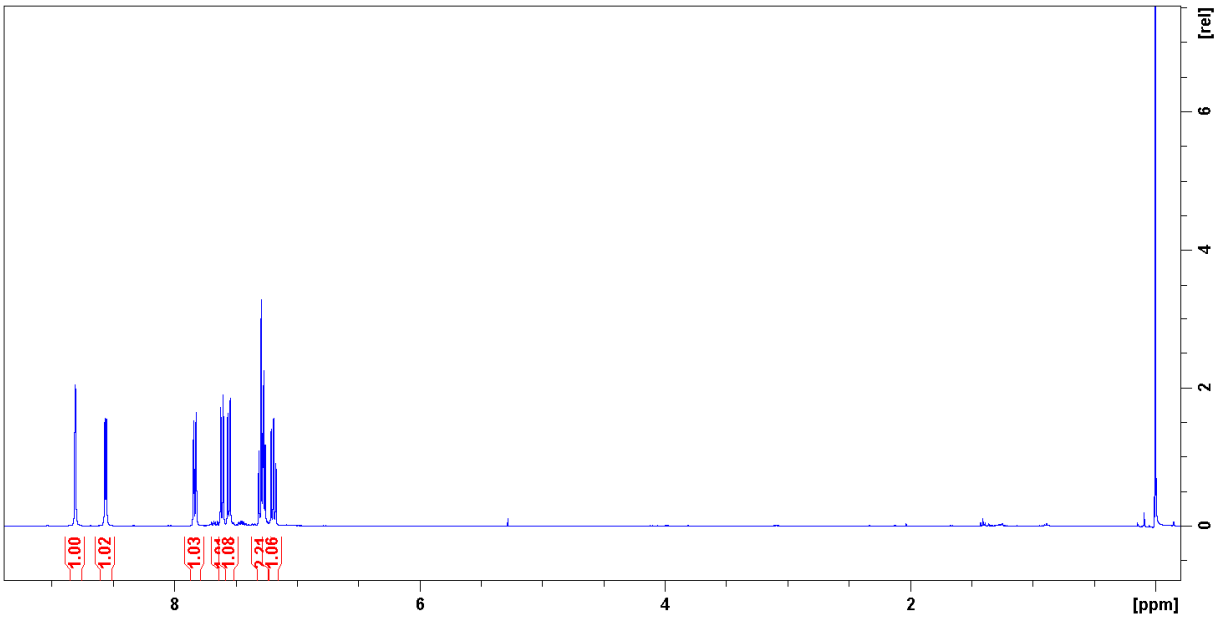

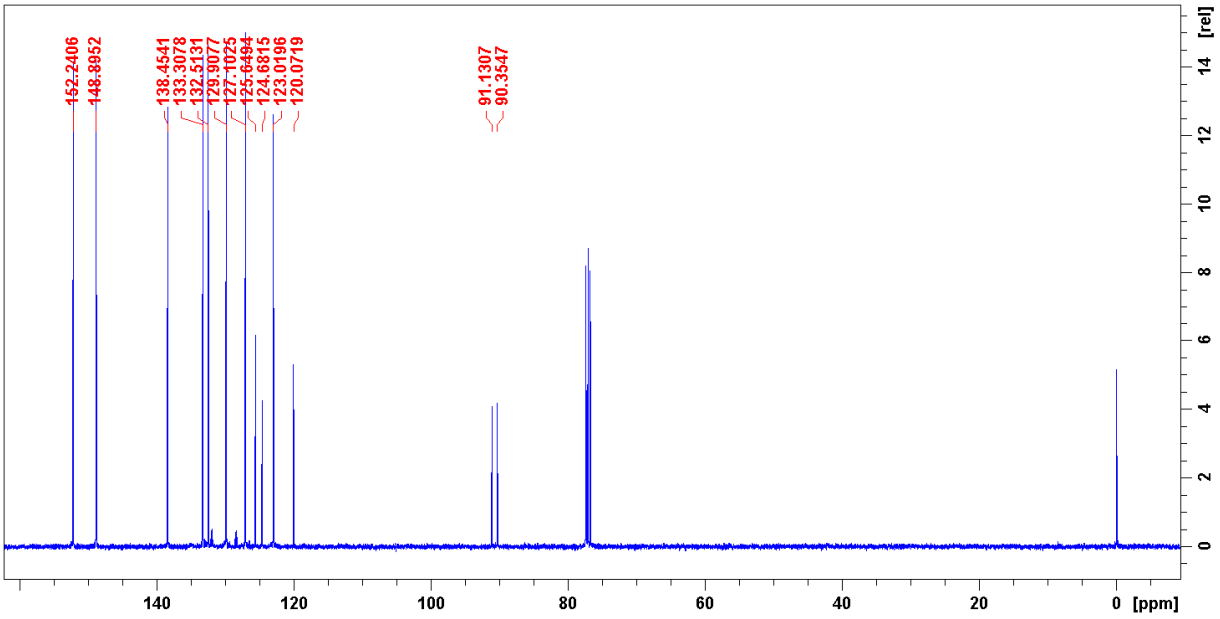

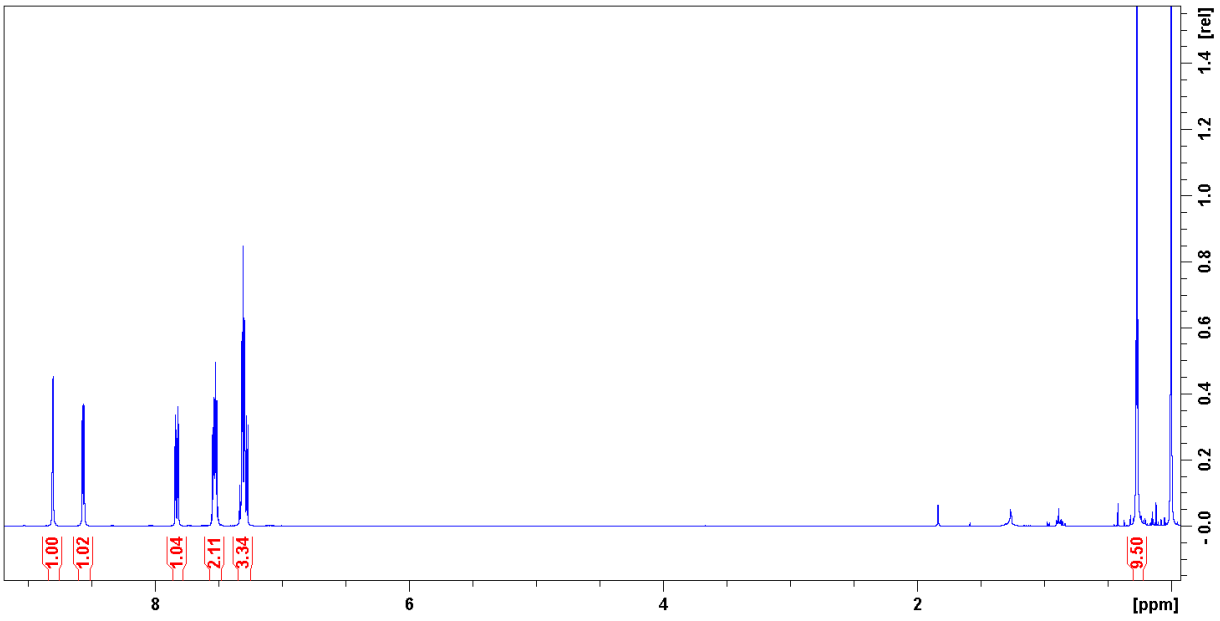

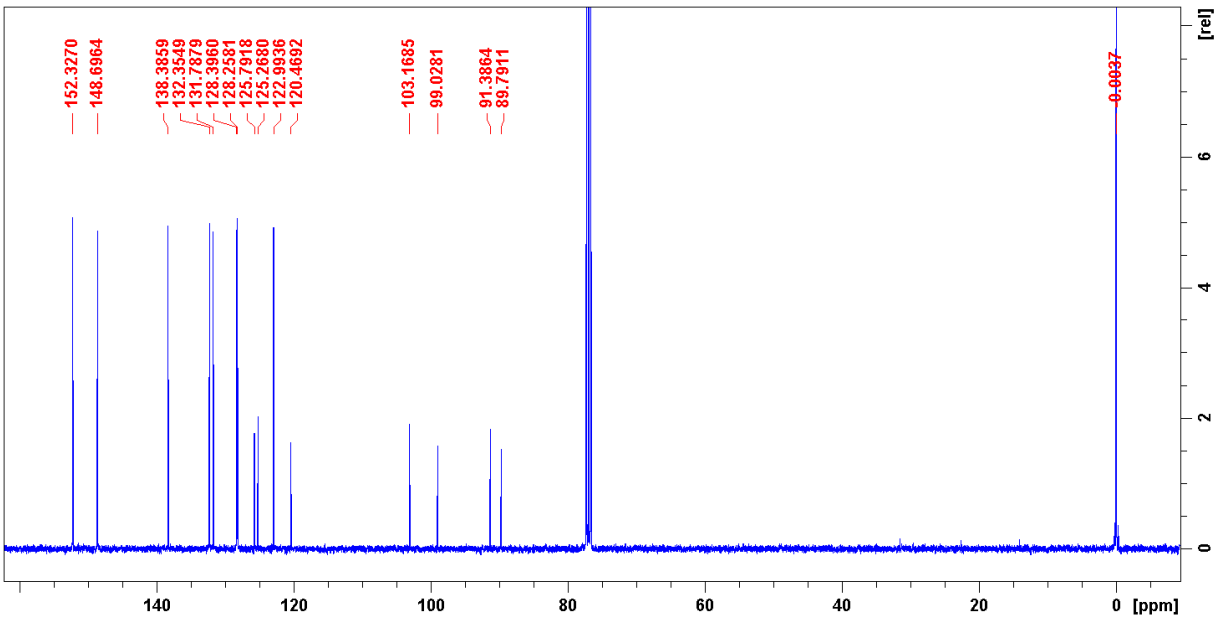

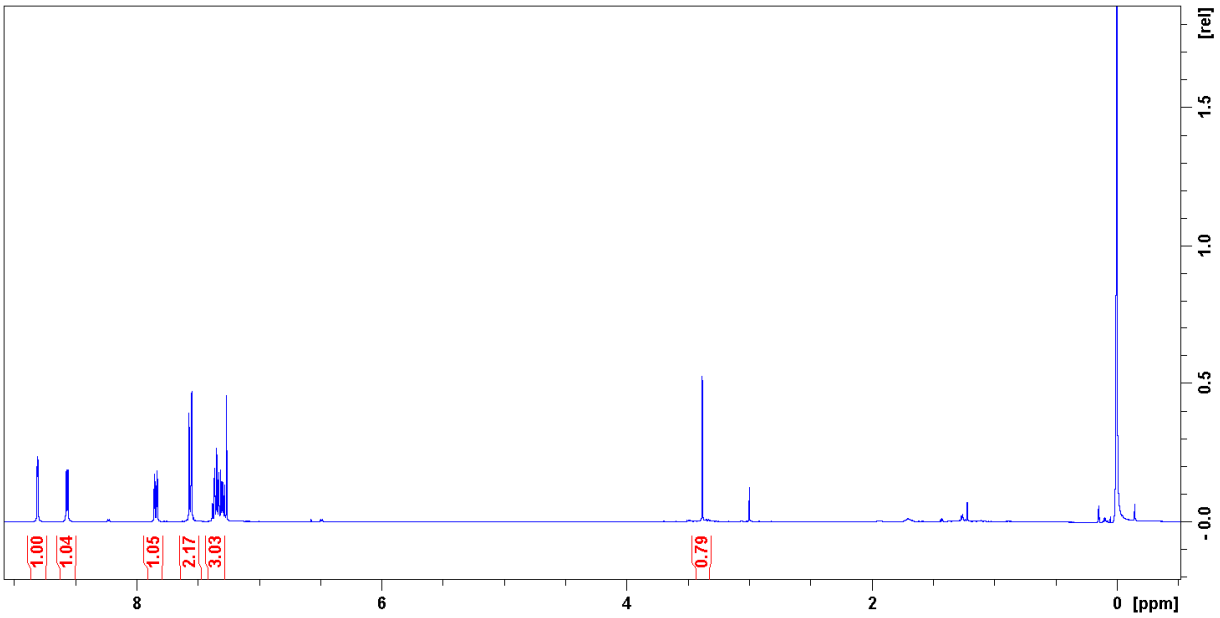

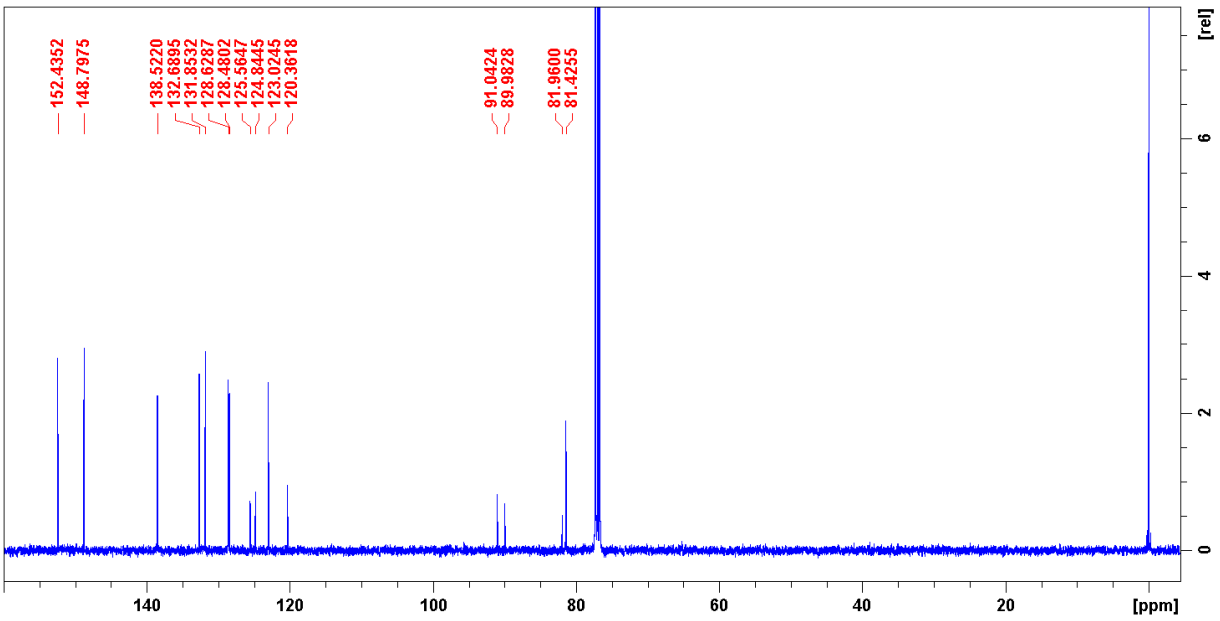

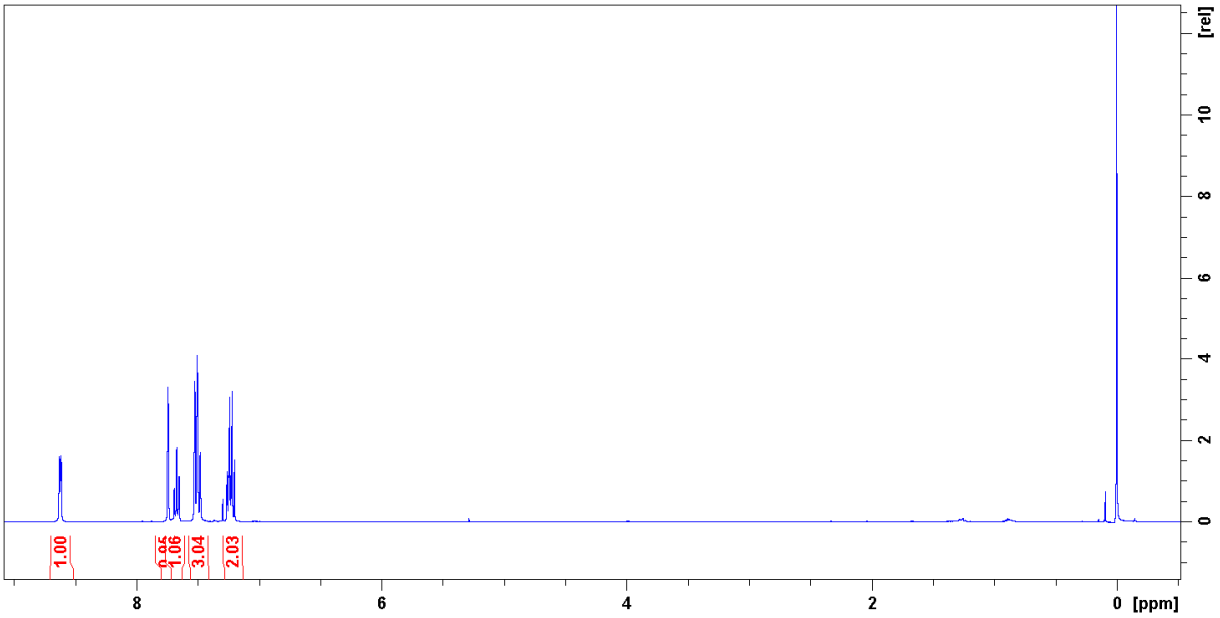

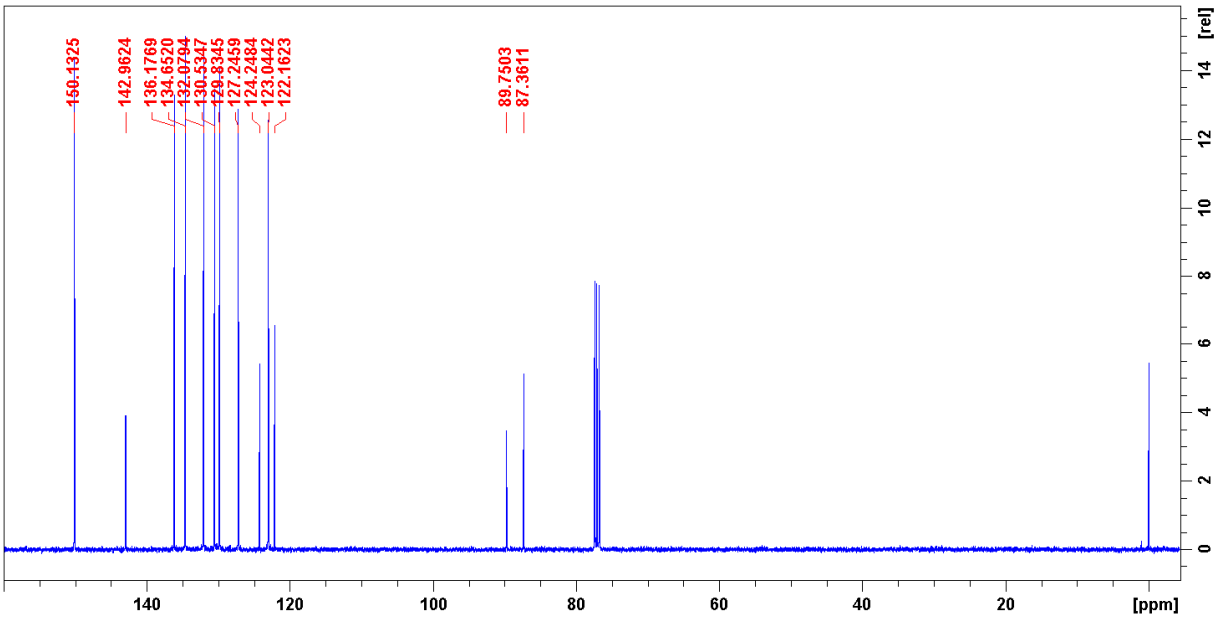

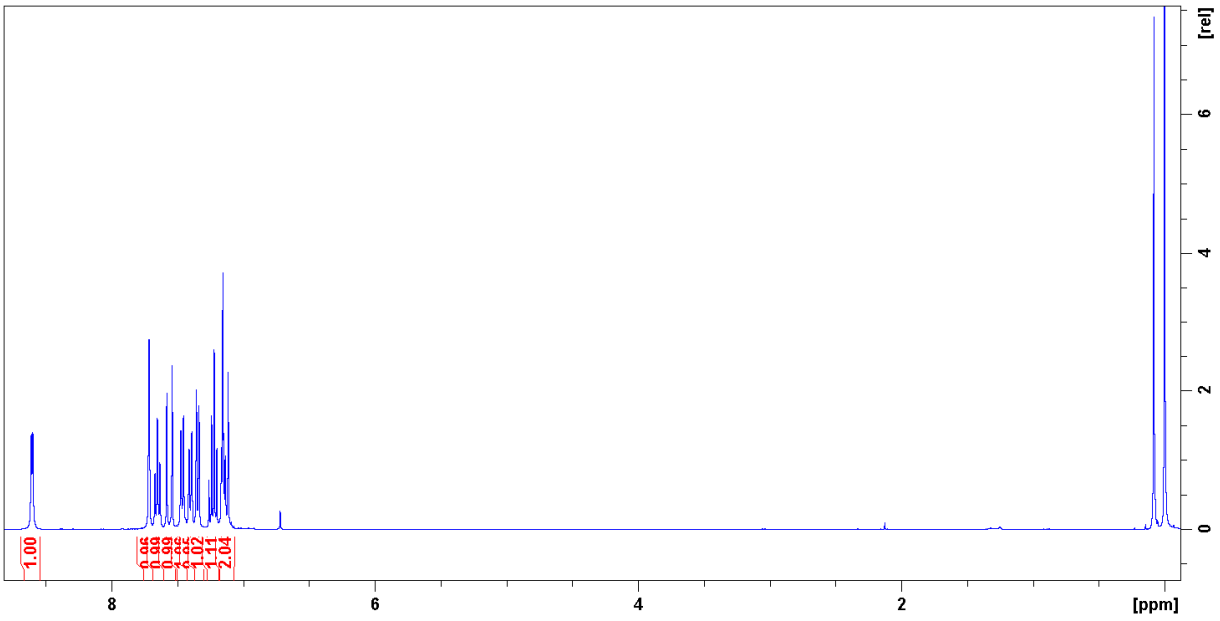

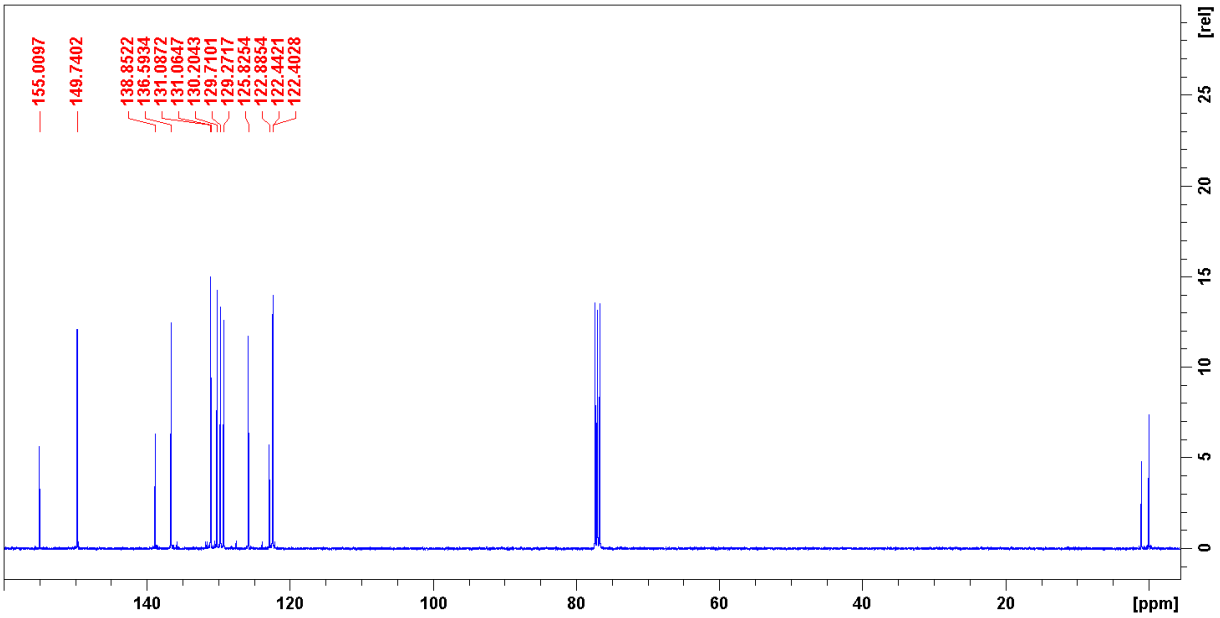

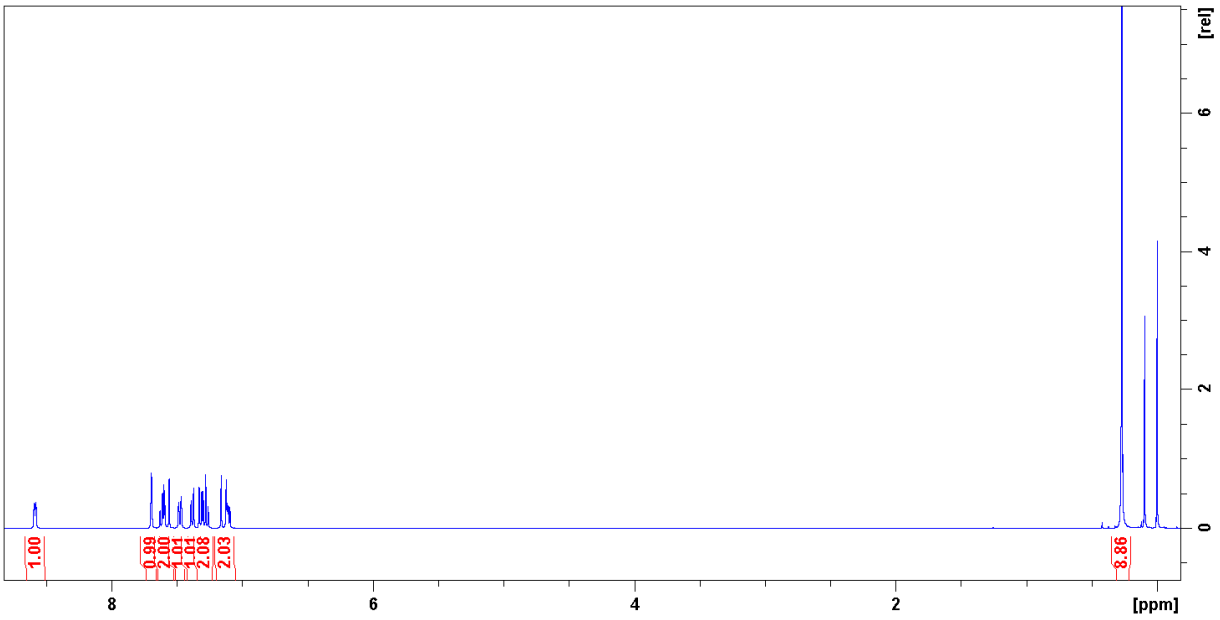

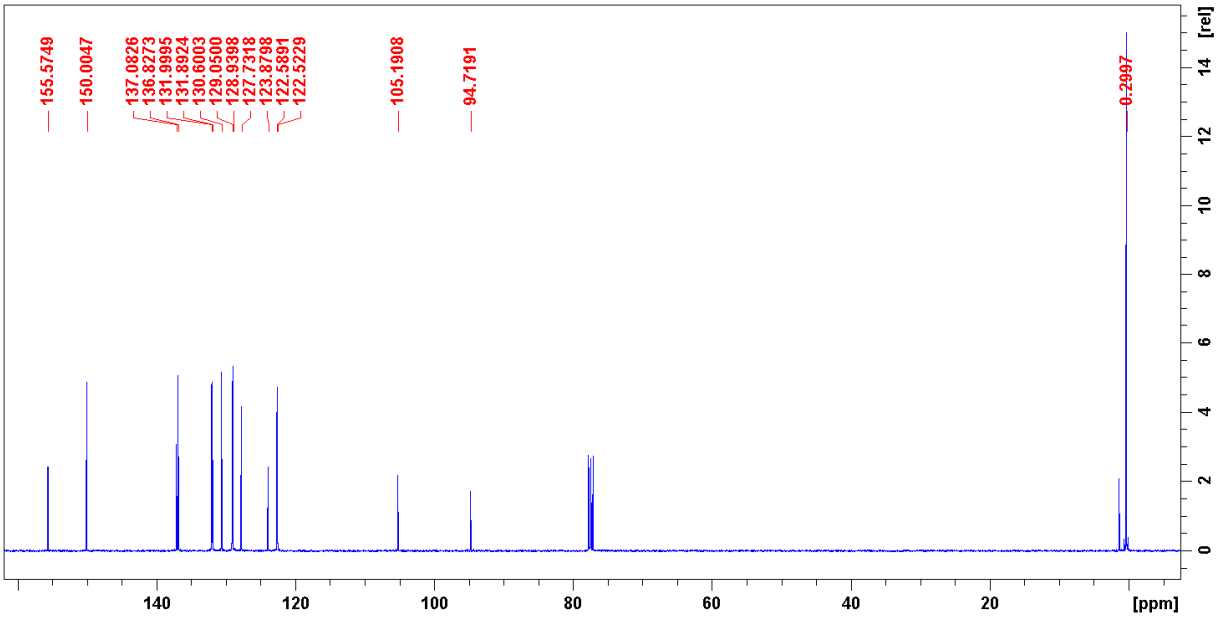

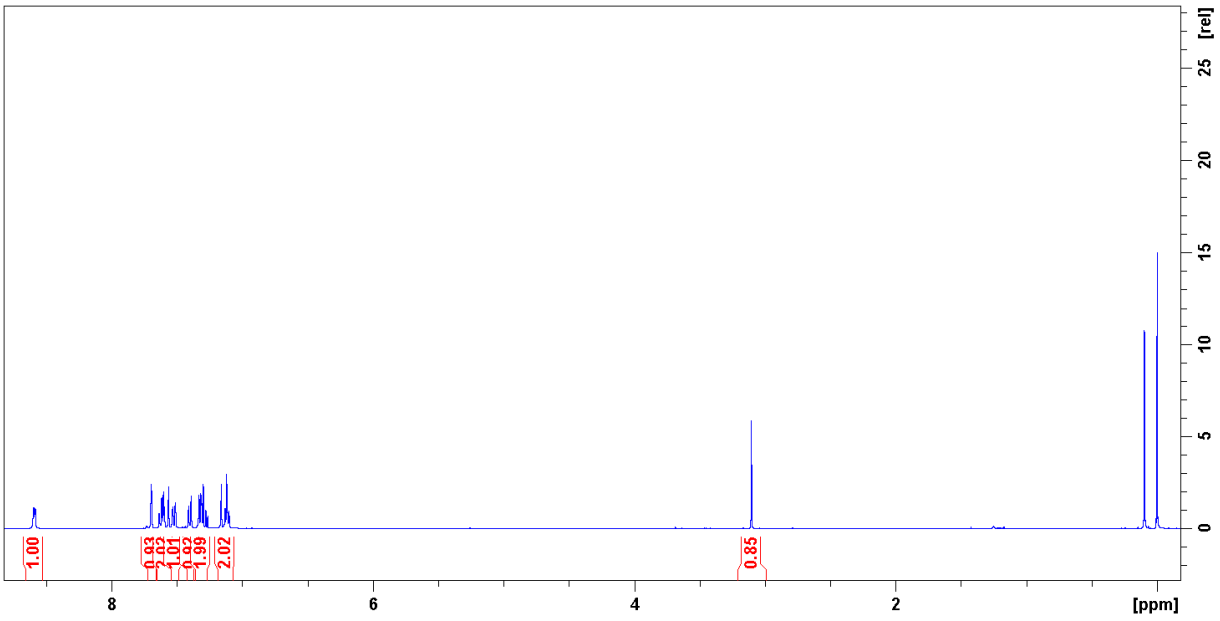

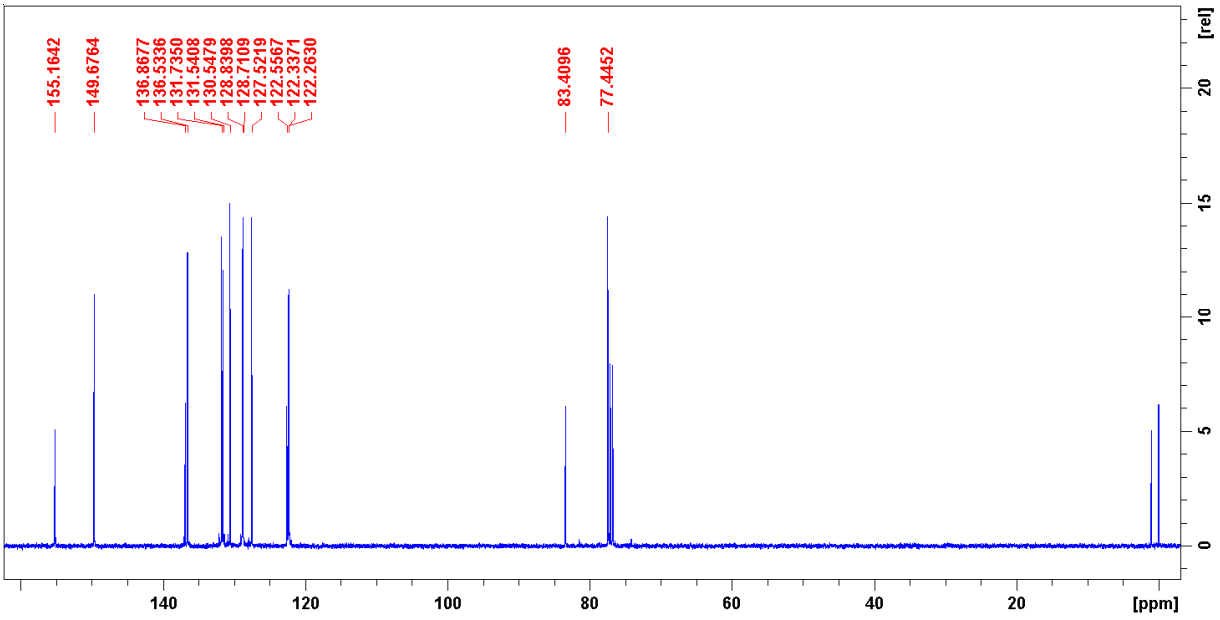

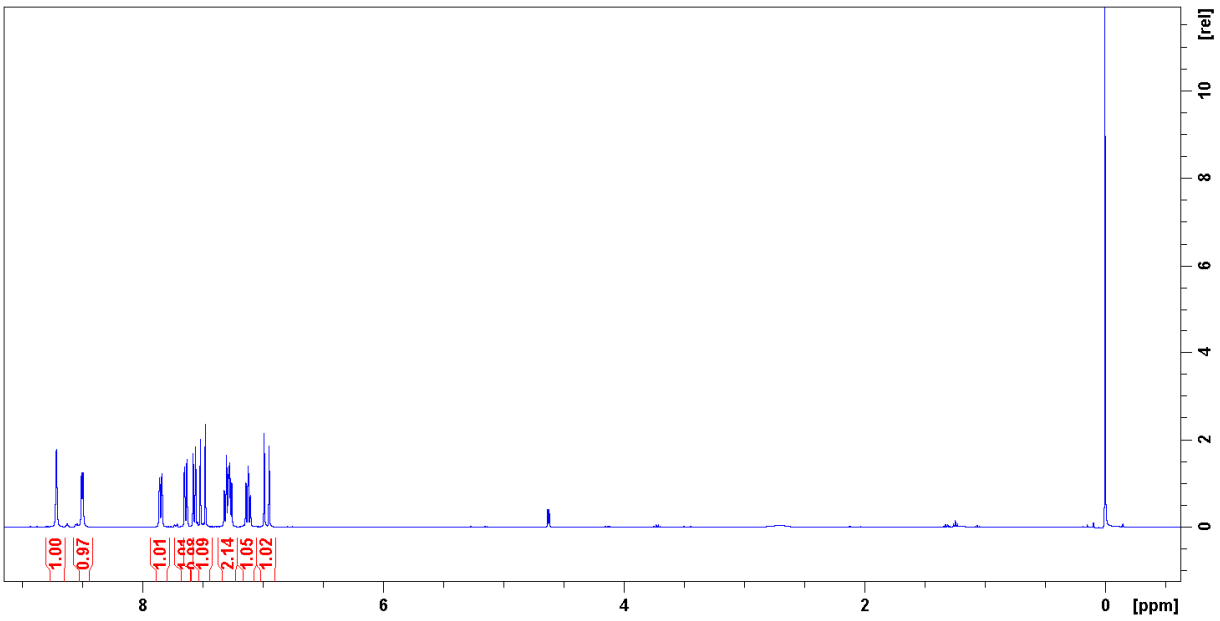

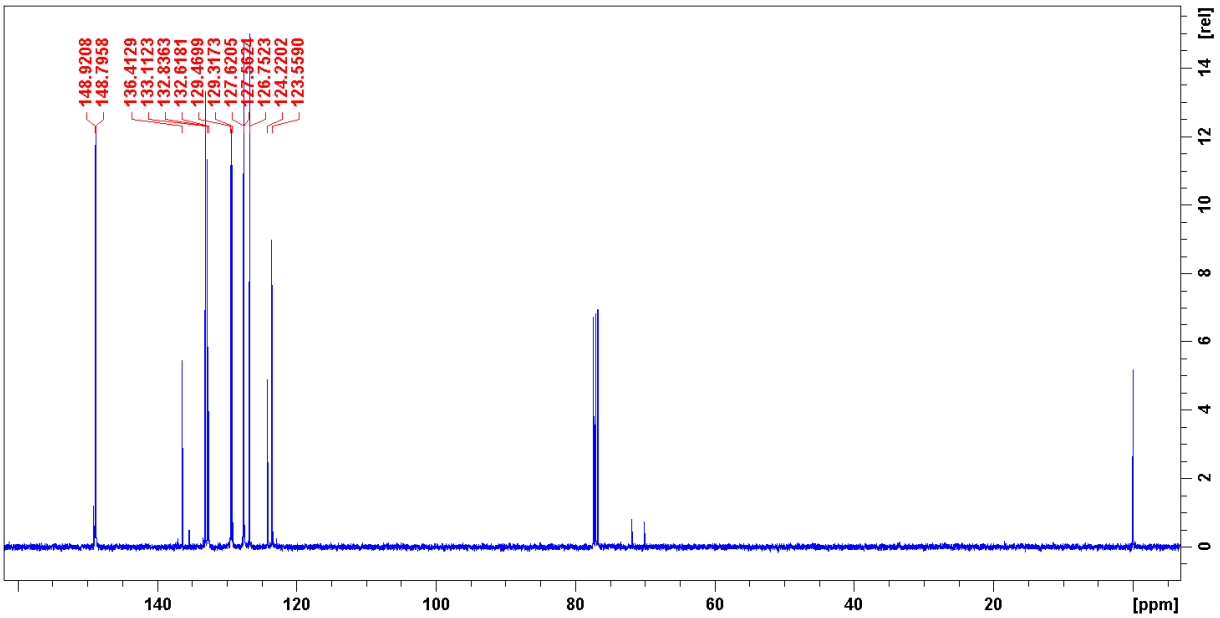

NMR Titration Studies

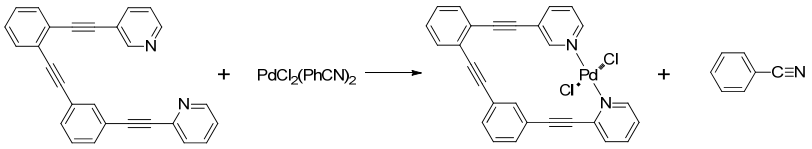

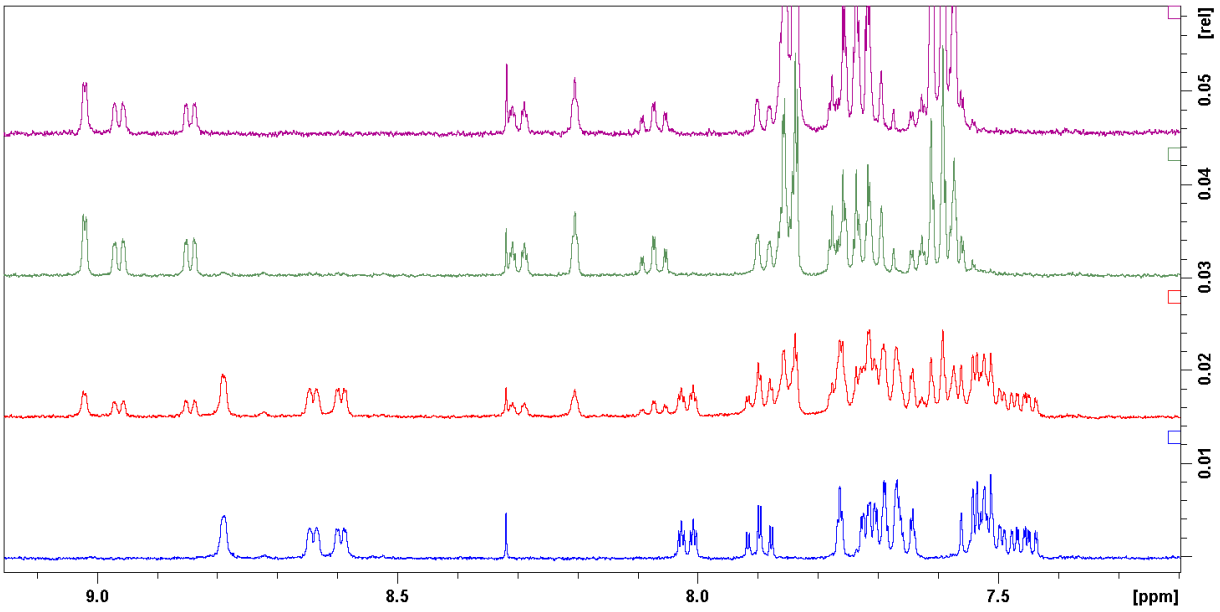

Figure S1. When $PdCl_2(PhCN)_2$ is introduced into a solution of ligand **1** in DMSO-d_6, signals for the ligand diminish while those for the Pd(II) complex (**1-Pd**) grow. The integration ratio is consistent with the mole fraction of Pd(II) introduced (A. 0.0 eq. $PdCl_2(PhCN)_2$, B. 0.35 eq. $PdCl_2(PhCN)_2$, C. 0.9 eq. $PdCl_2(PhCN)_2$, D. 3.3 eq. $PdCl_2(PhCN)_2$). This progression is consistent with stoichiometric binding of introduced Pd(II) by ligand **1**.

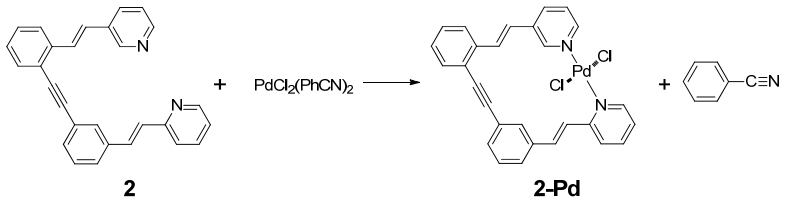

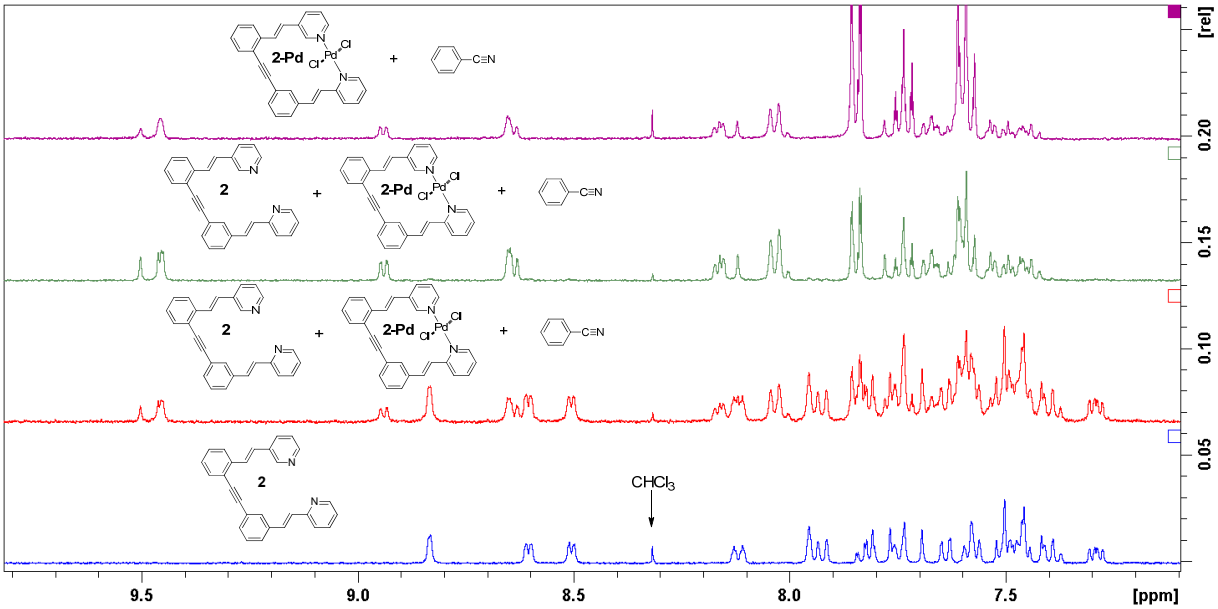

Figure S2. When $PdCl_2(PhCN)_2$ is introduced into a solution of ligand **2** in DMSO-d_6, signals for the ligand diminish while those for the Pd(II) complex (**2-Pd**) grow. The integration ratio is consistent with the mole fraction of Pd(II) introduced (A. 0.0 eq. $PdCl_2(PhCN)_2$, B. 0.35 eq. $PdCl_2(PhCN)_2$, C. 0.9 eq. $PdCl_2(PhCN)_2$, D. 3.2 eq. $PdCl_2(PhCN)_2$). This progression is consistent with stoichiometric binding of introduced Pd(II) by ligand **2**.

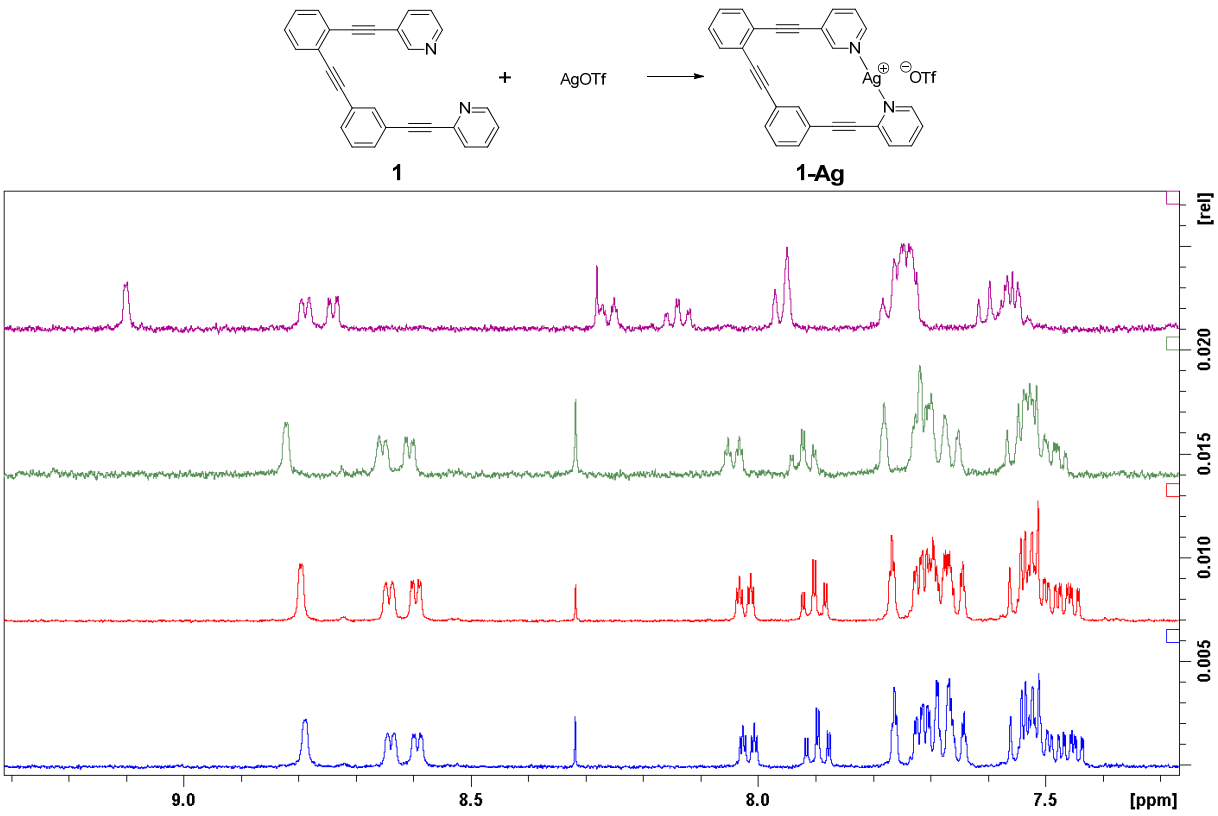

Figure S3. Introduction of AgOTf leads to gradual downfield shifting of resonances of ligand **1** (0.29-0.87 mM). An endpoint was reached by adding solid AgOTf (>400 eq) to the NMR tube.

Association constants were calculated by averaging K values derived from several different proton signals across several different trials. Trials in which samples were too concentrated (e.g. Trial #5), or in which there was a large excess of ligand (e.g. Trial #3) gave irreproducible results and were eliminated from consideration.

$$K = \frac{[\text{Complex}]}{([\text{Ligand 1}]-[\text{Complex}])\times([\text{Ag}]-[\text{Complex}])}$$

$$[\text{Complex}] = \frac{(H_{a(obs)}-H_{a(free)})}{(H_{a(complex)}-H_{a(free)})} \times [\text{Ligand 1}]$$

Table S1. Sample of data used to calculate K values from NMR titration experiments.

	[Ligand 1]	[Ag]	Chem. Shift Ha	δ Chem. Shift Ha	[Complex]	K
Trial #1	0.000291	0.000906	8.8216	0.0327	3.05E-05	133
Trial #2	0.000581	0.000604	8.8097	0.0208	3.88E-05	126
Trial #3	0.000872	0.000303	8.796	0.0071	1.99E-05	82.6
Trial #4	0.00157	0.00163	8.8413	0.0524	0.000264	148
Trial #5	0.00314	0.00326	8.8745	0.0856	0.000364	45.3
			Ha (free) = 8.7889			
			Ha (complex) = 9.1007			

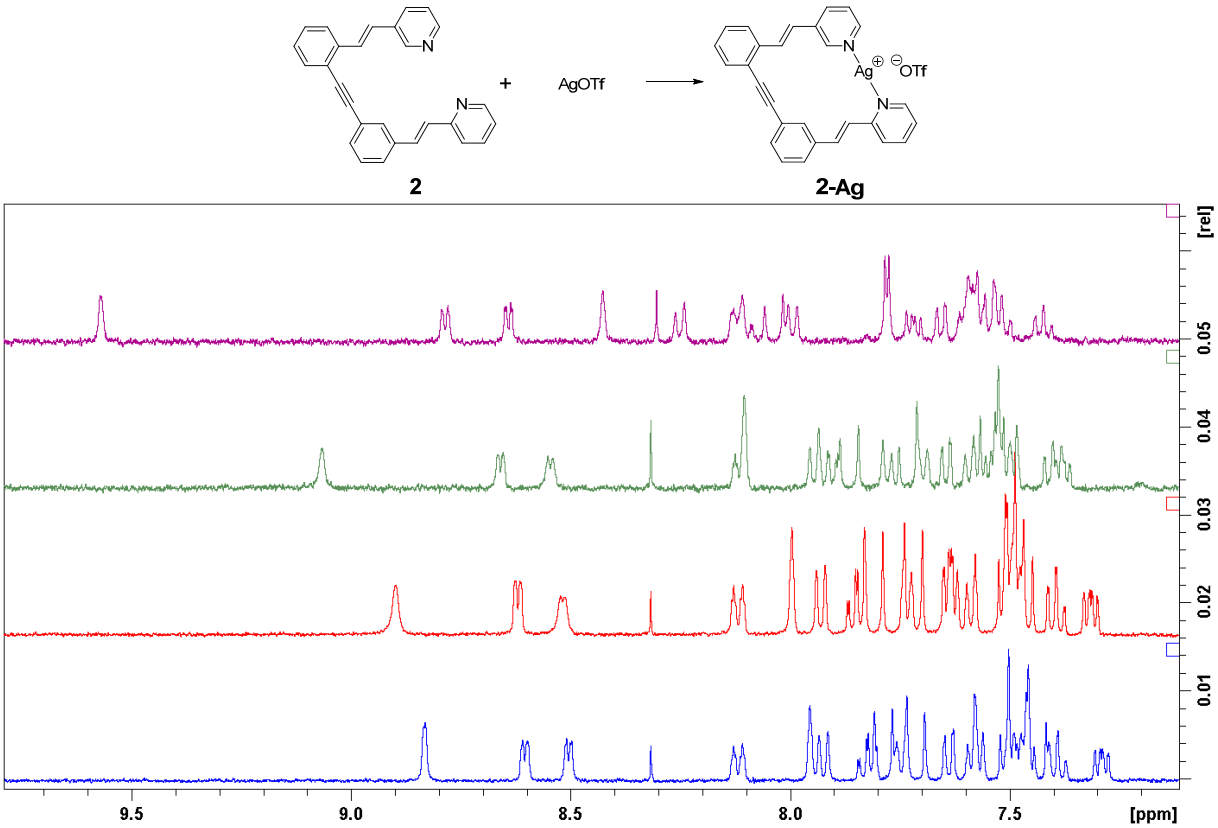

Figure S4. Introduction of AgOTf leads to gradual downfield shifting of ligand **2** (0.28-0.84 mM) resonances. Endpoints were reached by adding solid AgOTf (>150 eq) to the NMR tube.

Association constants were calculated by averaging K values derived from several different proton signals across several different trials. Trials in which samples were too concentrated (e.g. Trial #5), or in which there was a large excess of ligand (e.g. Trial #3) gave irreproducible results and were eliminated from consideration.

$$K = \frac{[\text{Complex}]}{([\text{Ligand 2}]-[\text{Complex}])\times([\text{Ag}]-[\text{Complex}])}$$

$$[\text{Complex}] = \frac{(H_{a(obs)}-H_{a(free)})}{(H_{a(complex)}-H_{a(free)})}\times[\text{Ligand 2}]$$

Table S2. Sample of data used to calculate K values from NMR titration experiments.

	[Ligand 2]	[Ag]	Chem. Shift Ha	δ Chem. Shift Ha	[Complex]	K
Trial #1	0.00028	0.000906	9.068	0.234	8.87E-05	568
Trial #2	0.000559	0.000604	8.987	0.153	0.000116	536
Trial #3	0.000839	0.000302	8.9	0.066	7.50E-05	432
Trial #4	0.00151	0.00163	9.1116	0.2776	0.000568	567
Trial #5	0.00302	0.00326	9.219	0.385	0.00158	647
			Ha (free) = 8.834			
			Ha (complex) = 9.572			

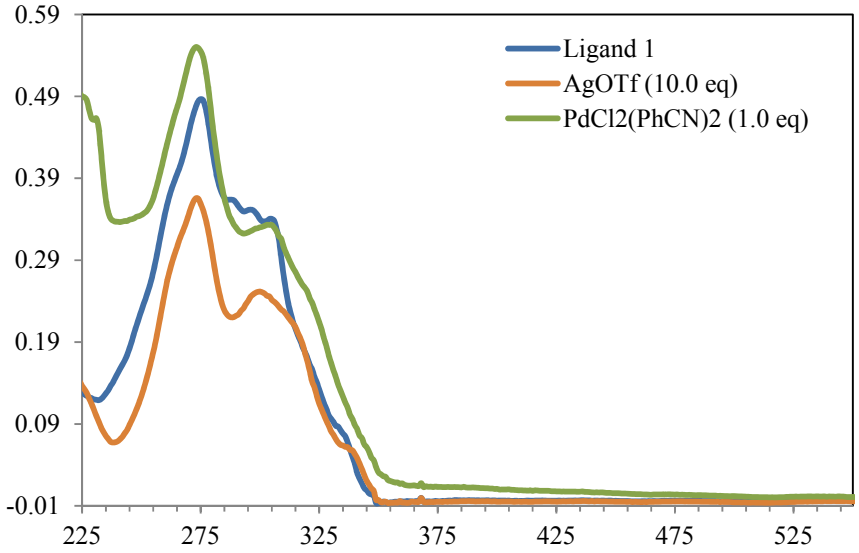

Figure S5. Introduction of either AgOTf or $PdCl_2(PhCN)_2$ to ligand **1** (8.5×10^{-6} M in THF) leads to no significant changes to the observed λ_{max}'s in the electronic absorbance profile of the ligand. The only differences observed between complexed and uncomplexed ligand are small changes in molar absorptivity and the absorbance spectra of the Pd(II) complexes tailing into the visible region, giving the complex an orange appearance.

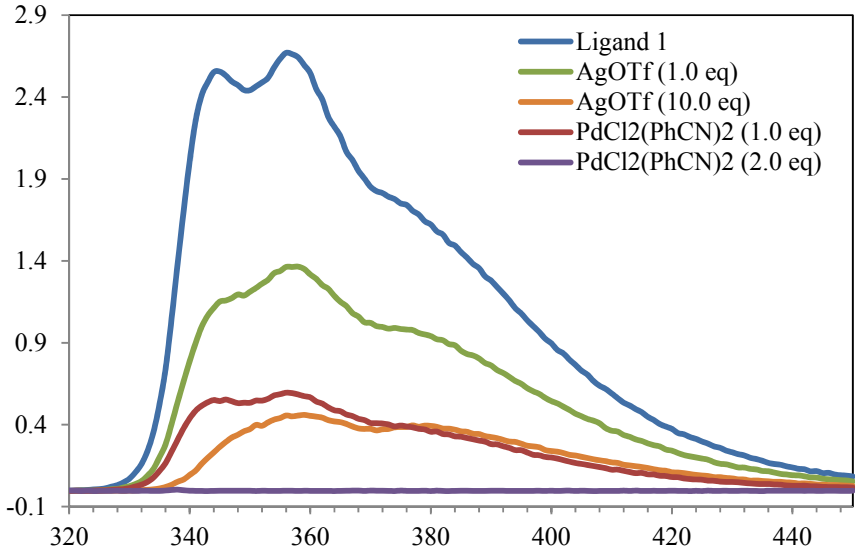

Figure S6. Introduction of AgOTf leads to the gradual quenching of the fluorescence of ligand **1** (8.5×10^{-6} M in THF, $\lambda_{exc} = 307$ nm) with decreasing signal intensity as more Ag(I) is added. $PdCl_2(PhCN)_2$ leads to efficient fluorescence quenching, with no fluorescence observed with two equivalents of Pd(II) added. The quenching efficiency of each metal is consistent with the relative binding strengths of Ag(I) and Pd(II) cations to ligand **1**.

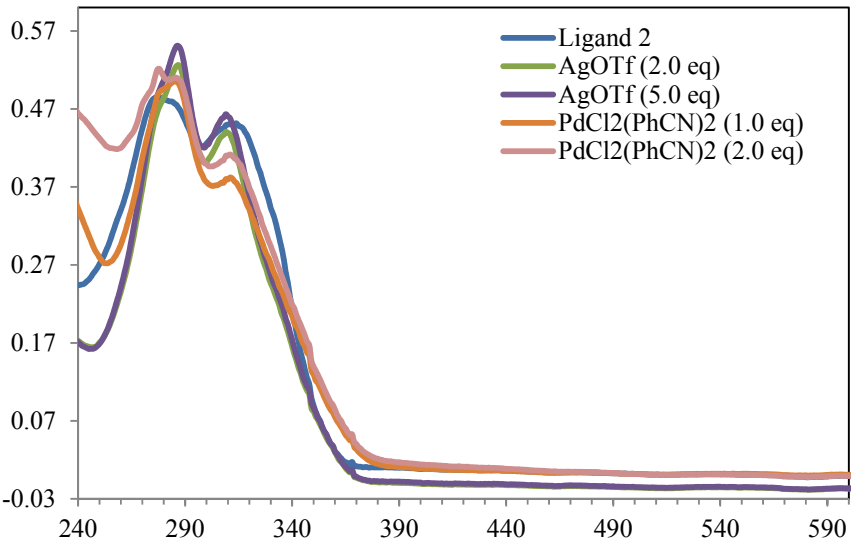

Figure S7. Introduction of either AgOTf or $PdCl_2(PhCN)_2$ to ligand **2** (8.2×10^{-6} M in THF) leads to no significant changes to the observed λ_{max}'s in the electronic absorbance profile of the ligand. The only differences observed between complexed and uncomplexed ligand are small changes in molar absorptivity and the absorbance spectra of the Pd(II) complexes tailing into the visible region, giving the complex an orange appearance.

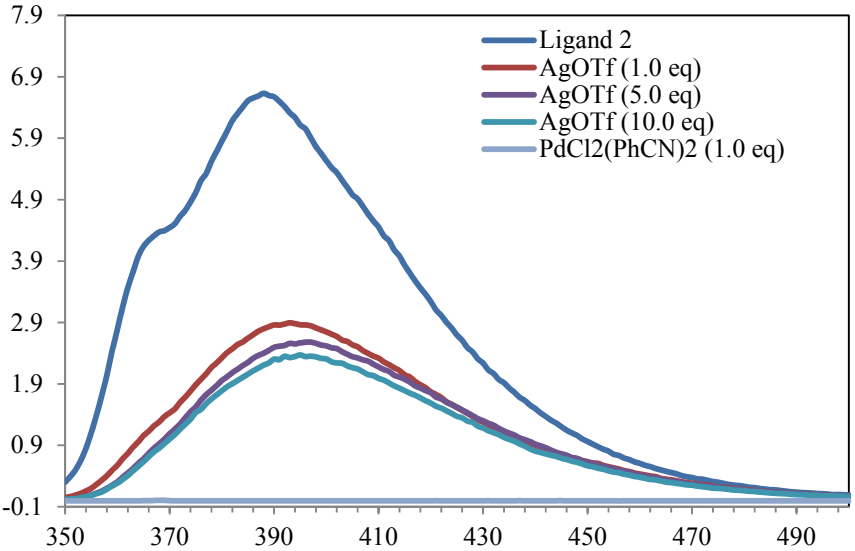

Figure S8. Introduction of AgOTf leads to the gradual quenching of the fluorescence of ligand **2** (8.2×10^{-6} M in THF, $\lambda_{exc} = 332$ nm) with decreasing signal intensity as more Ag(I) is added. $PdCl_2(PhCN)_2$ leads to efficient fluorescence quenching, with no fluorescence observed with one equivalent of Pd(II) added. The quenching efficiency of each metal is consistent with the relative binding strengths of Ag(I) and Pd(II) cations to ligand **2**.

Table S3. Crystal data for ligand **1** and coordination complexes of ligand **1**.

complex	**1**	**1**· $AgC_2F_3O_2$	**1**·$PdCl_2$·CH_2Cl_2
Formula	$C_{28}H_{16}N_2$	$C_{30}H_{16}Ag\ F_5N_2O_2$	$C_{29}H_{18}\ N_2PdCl_4$
M/g mol^{-1}	380.43	601.32	642.65
crystal system	monoclinic	monoclinic	triclinic
space group	P21/c	P21/n	P-1
a/Å	12.7773(14)	16.8364(17)	8.5163(5)
b/Å	14.4079(15)	7.9149(8)	11.2205(6)
c/Å	12.3216(13)	19.851(2)	14.9946(12)
α/°	90	90	102.112(1)
β/°	117.4760(10)	114.2540(10)	95.543(1)
γ/°	90	90	107.875(1)
V/ $Å^3$	2012.5(4)	2411.8(4)	1313.21(15)
Z	4	4	2
$\rho_{calcd.}$/g cm^{-3}	1.256	1.656	1.625
μ/mm^{-1}	1.061	0.891	1.136
F(0,0,0)	792	1200.0	640.0
Crystal size, mm	0.28×0.20×0.13	0.40×0.07×0.04	0.40×0.20×0.20
Temp./K	173(2)	173(2)	173(2)
θ range/°	1.8-27.2	1.3-27.2	1.4-27.2
Reflections Collected	23414	27258	15308
Independent Reflections	4482	5356	5797
Data/restraints/ parameters	4482/0/271	5356/0/343	5797/0/325
Goof	1.005	1.008	1.065
R(int)	0.058	0.088	0.014
Final R indices[I>2σ(I)], R1/wR2	0.045/0.115	0.047/0.104	0.020/0.053
Largest diff. peak/hole /e$Å^3$	0.16/-0.18	0.83/-0.90	0.52/-0.68

Table S4. Crystal data for coordination complexes of ligand **2**.

complex	**2**· $AgCF_3SO_3 \cdot CH_3OH$	**2**·$PdCl_2$
Formula	$C_{30}H_{24}AgF_3N_2O_4S$	$C_{28}H_{20}N_2PdCl_2$
M/g mol^{-1}	673.45	561.76
crystal system	monoclinic	orthorhombic
space group	P21/c	PFddd
a/Å	7.5430 (9)	16.0921(13)
b/Å	18.135 (2)	27.4790(13)
c/Å	20.575 (3)	44.234(3)
α/°	90	90
β/°	95.252 (4)	90
γ/°	90	90
V/ $Å^3$	2802.7 (6)	19560(2)
Z	4	32
$\rho_{calcd.}$/g cm^{-3}	1.656	1.526
μ/mm^{-1}	0.85	0.996
F(0,0,0)	1360.0	9024.0
Crystal size, mm	0.60×0.10×0.06	0.29×0.20×0.05
Temp./K	200	173(2)
θ range/°	2.9-17.6	2.6-27.0
Reflections Collected	43347	55436
Independent Reflections	4958	5472
Data/restraints/ parameters		5472/0/298
Goof	1.046	1.087
R(int)	0.093	0.041
Final R indices[I>2σ(I)], R1/wR2	0.041/0.104	0.026/0.068
Largest diff. peak/hole /e$Å^3$	0.59/-0.55	0.45/-0.32

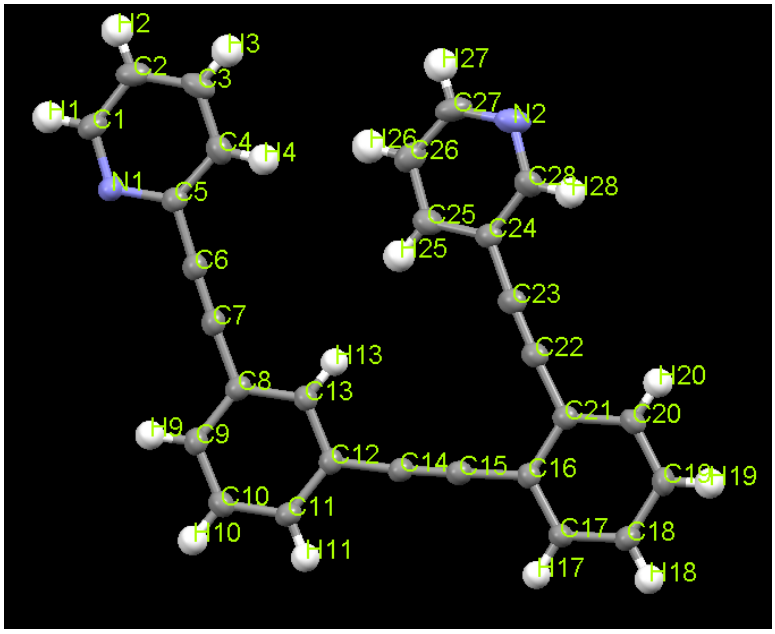

Table S5. Select Bond Lengths, Bond Angles and Torsional Angles for Ligand **1**

Bond Lengths (Å)

N1-C5	1.348(2)	C14-C15	1.196(2)
C4-C5	1.389(2)	C16-C21	1.413(2)
C5-C6	1.437(2)	C21-C22	1.432(2)
C6-C7	1.200(2)	C22-C23	1.199(2)
C8-C13	1.395(2)	C24-C25	1.387(2)
C12-C14	1.437(2)	N2-C28	1.327(2)

Bond Angles (deg)

N1-C5-C6	116.48(15)	C21-C16-C15	119.96(14)
C7-C6-C5	178.33(18)	C16-C21-C22	121.32(14)
C6-C7-C8	177.88(18)	C23-C22-C21	177.03(18)
C13-C8-C7	119.08(15)	C22-C23-C24	176.53(18)
C13-C12-C14	118.74(15)	C28-C24-C23	119.66(15)
C15-C14-C12	175.75(17)	C28-N2-C27	116.36(16)
C14-C15-C16	175.98(17)		

Torsional Angles (deg)

N1-C5-C8-C9	-14.54	C11-C12-C16-C17	1.49
C4-C5-C8C13	-13.50	C16-C21-C24-C25	-15.01
C13-C12-C16-C21	4.06	C20-C21-C24-C28	-14.01

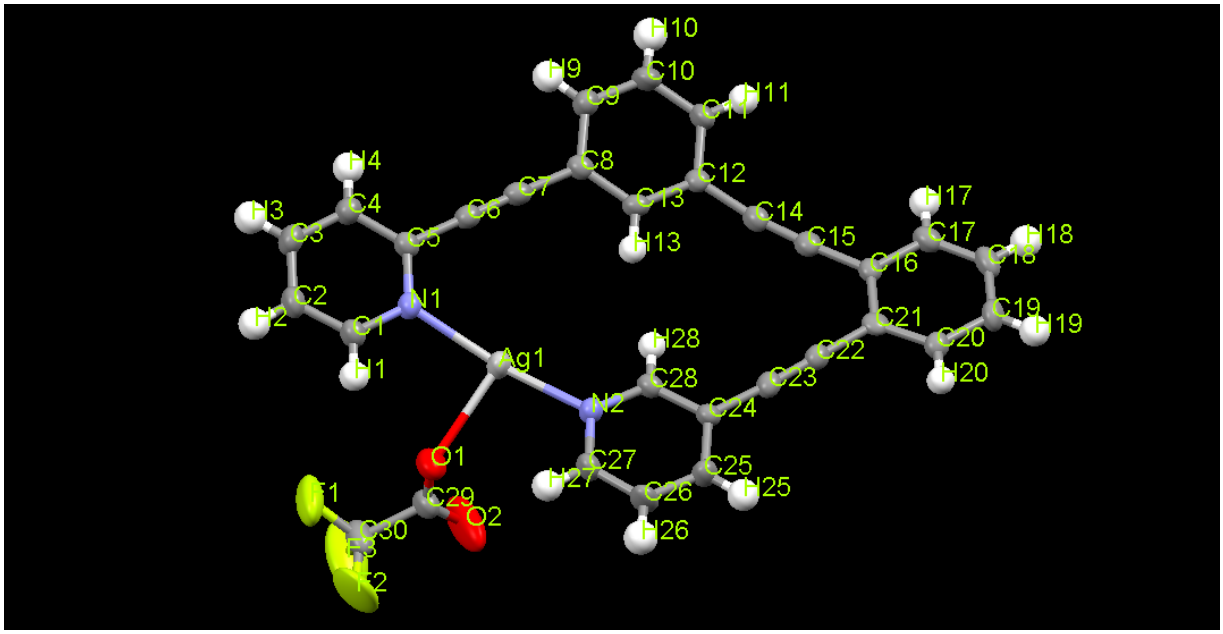

Table S6. Select Bond Lengths, Bond Angles and Torsional Angles for **CF_3CO_2[1·Ag]**

Bond Lengths (Å)

Ag1-N2	2.188(3)	C12-C14	1.435(6)
Ag1-N1	2.197(3)	C14-C15	1.199(6)
Ag1-O1	2.514(3)	C16-C21	1.406(5)
N1-C5	1.355(5)	C21-C22	1.449(6)
C5-C6	1.436(6)	C22-C23	1.185(5)
C6-C7	1.191(6)	C24-C25	1.393(6)

Bond Angles (deg)

N2-Ag1-N1	165.07(13)	C13-C8-C7	119.8(4)
N2-Ag1-O1	93.85(12)	C15-C14-C12	171.7(5)
N1-Ag1-O1	89.95(12)	C14-C15-C16	174.4(5)
C5-N1-Ag1	124.2(3)	C21-C16-C15	121.3(4)
N1-C5-C6	116.7(4)	C23-C22-C21	179.1(5)
C7-C6-C5	179.2(5)	C22-C23-C24	176.8(5)
C6-C7-C8	177.1(5)	C28-C24-C23	118.9(4)

Torsional Angles (deg)

C1-N1-Ag1-O1	8.46	C4-C5-C8-C9	5.91
C27-N2-Ag1-O1	-12.17	C13-C12-C16-C21	-12.61
C1-N1-N2-C27	-4.33	C11-C12-C16-C17	-11.68
C5-N1-N2-C28	-0.58	C16-C21-C24-C28	-6.93
N1-C5-C8-C13	2.13	C20-C21-C24-C25	-6.51

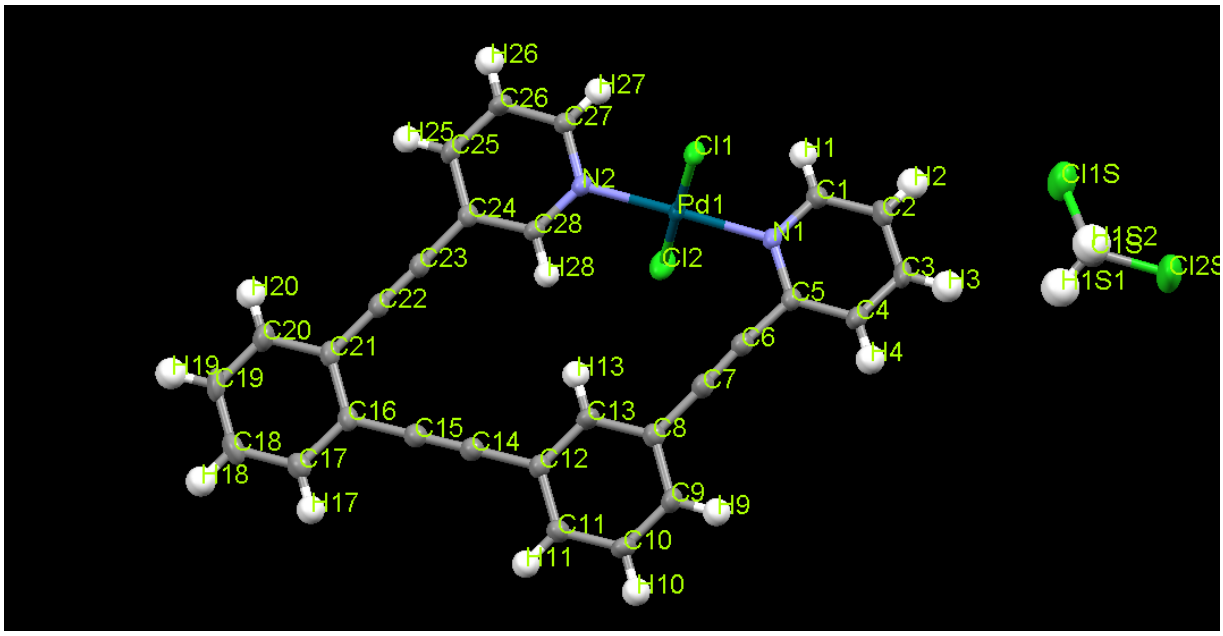

Table S7. Select Bond Lengths, Bond Angles and Torsional Angles for **1·PdCl$_2$·CH$_2$Cl$_2$**

Bond Lengths (Å)

Pd1-N1	2.0217(13)	C12-C14	1.435(2)
Pd1-N2	2.0243(13)	C14-C15	1.194(3)
Pd1-Cl2	2.2754(4)	C22-C23	1.194(2)
N1-C5	1.355(2)	C23-C24	1.433(2)
C5-C6	1.428(2)	C24-C28	1.396(2)
C6-C7	1.192(2)	N2-C28	1.341(2)

Bond Angles (deg)

N1-Pd1-N2	176.49(5)	C15-C14-C12	178.2(2)
N1-Pd1-Cl2	88.96(4)	C14-C15-C16	179.4(2)
N1-Pd1-Cl1	90.22(4)	C16-C21-C22	120.47(15)
C5-N1-Pd1	121.84(11)	C23-C22-C21	178.83(19)
C7-C6-C5	173.96(19)	C22-C23-C24	176.76(19)
C6-C7-C8	176.45(19)	C28-C24-C23	120.03(15)
C13-C12-C14	120.39(15)	C28-N2-Pd1	120.48(11)

Torsional Angles (deg)

Cl1-Pd1-N2-C27	69.63	C4-C5-C8-C9	-1.21
Cl1-Pd1-N1-C1	-81.53	C11-C12-C16-C17	4.18
C1-N1-N2-C27	-11.81	C13-C12-C16-C21	0.95
C5-N1-N2-C28	-12.42	C16-C21-C24-C28	-2.74
N1-C5-C8-C13	-1.23	C20-C21-C24-C25	0.81

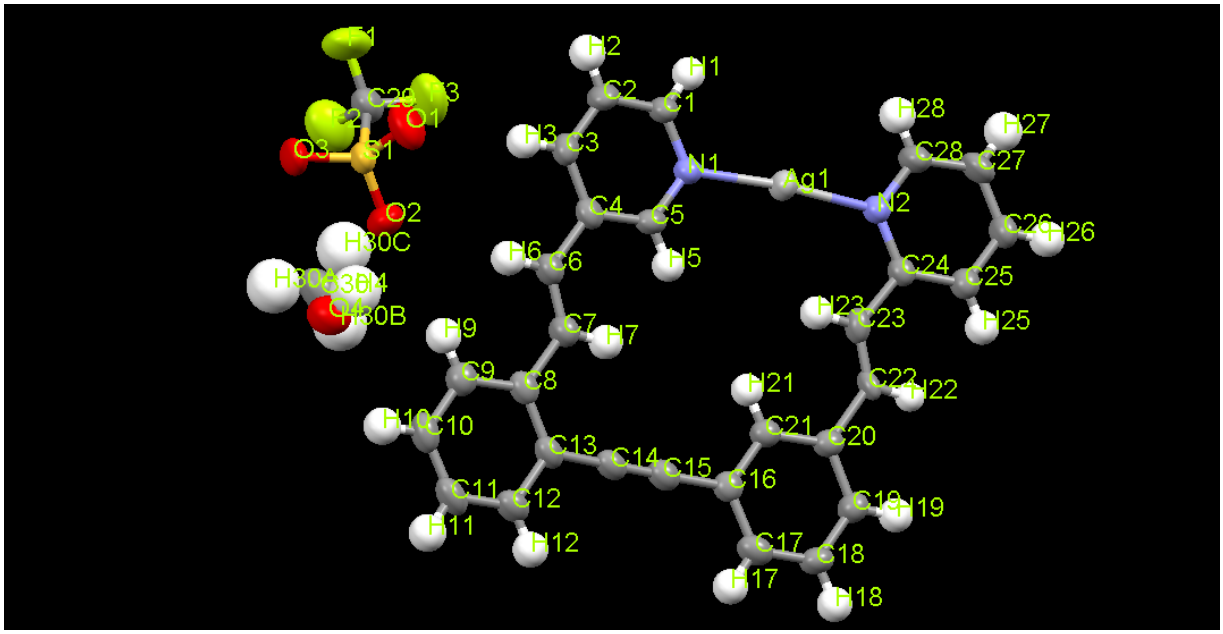

Table S8. Select Bond Lengths, Bond Angles and Torsional Angles for **2·AgOTf·CH$_3$OH**

Bond Lengths (Å)

Ag1-N1	2.127(3)	C13-C14	1.437(5)
Ag1-N2	2.141(3)	C14-C15	1.193(5)
N1-C5	1.356(4)	C20-C21	1.389(5)
C4-C6	1.477(5)	C20-C22	1.520(4)
C6-C7	1.284(5)	C22-C23	1.220(5)
C8-C13	1.401(5)	C23-C24	1.489(5)

Bond Angles (deg)

N1-Ag1-N2	174.66(10)	C14-C15-C16	178.0(4)
C1-N1-C5	117.6(3)	C21-C16-C15	119.9(3)
C5-C4-C6	122.9(3)	C21-C20-C22	120.6(3)
C7-C6-C4	127.3(3)	C23-C22-C20	130.0(3)
C6-C7-C8	127.8(4)	C22-C23-C24	126.6(3)
C13-C8-C7	119.4(3)	C25-C24-C23	122.3(3)
C15-C14-C13	178.8(4)	N2-C24-C23	116.8(3)

Torsional Angles (deg)

C5-N1-N2-C24	-2.79	C8-C13-C16-C21	0.15
C1-N1-N2-C28	1.27	C12-C13-C16-C17	-3.25
C3-C4-C8-C9	0.76	C21-C20-C24-N2	-2.08
C5-C4-C8-C13	0.57	C19-C20-C24-C25	-0.25

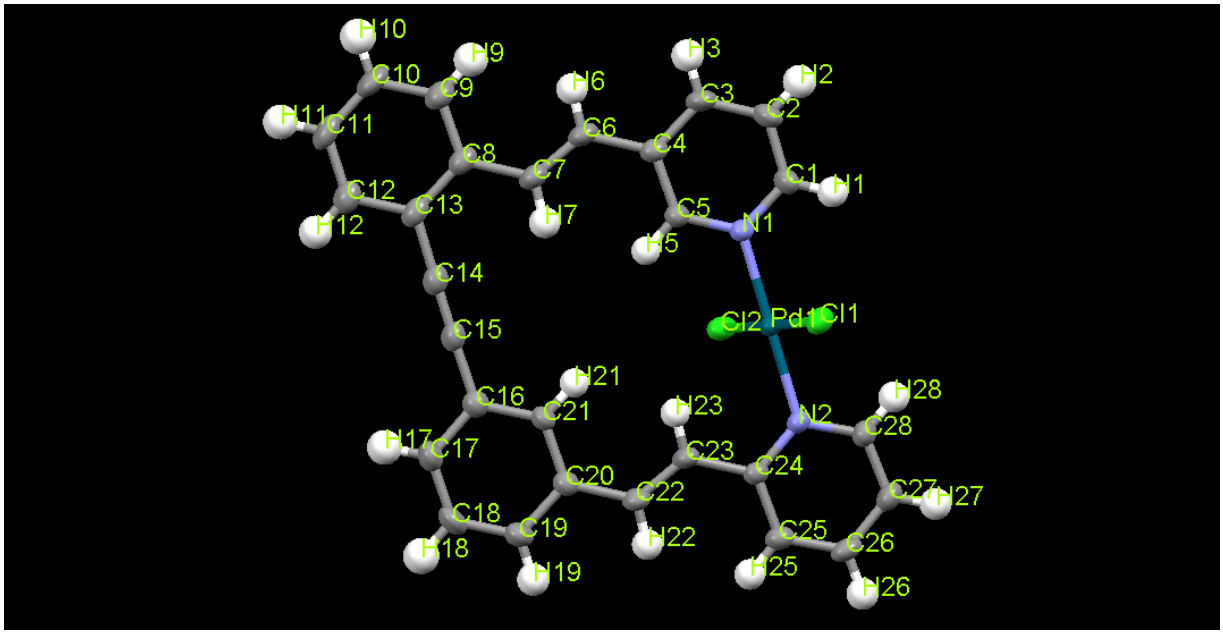

Table S9. Select Bond Lengths, Bond Angles and Torsional Angles for **2·PdCl$_2$**

Bond Lengths (Å)

Pd1-N1	2.0153(18)	C6-C7	1.315(4)
Pd1-N2	2.0281(18)	C7-C8	1.469(3)
Pd1-Cl1	2.3026(6)	C13-C14	1.432(3)
Pd1-Cl2	2.3077(6)	C14-C15	1.195(3)
N1-C5	1.337(3)	C20-C22	1.463(3)
C4-C6	1.467(3)	C22-C23	1.303(3)

Bond Angles (deg)

N1-Pd1-N2	179.82(9)	C15-C14-C13	179.4(3)
N1-Pd1-Cl1	90.53(6)	C14-C15-C16	178.6(3)
N1-Pd1-Cl2	88.38(6)	C21-C16-C15	120.6(2)
C1-N1-Pd1	120.53(15)	C21-C20-C22	122.1(2)
C5-C4-C6	122.4(2)	C23-C22-C20	126.7(2)
C7-C6-C4	126.9(2)	C22-C23-C24	126.6(2)
C6-C7-C8	126.8(2)	N2-C24-C23	117.51(19)

Torsional Angles (deg)

Cl1-Pd1-N1-C5	-114.33	C5-C4-C8-C13	-1.50
Cl1-Pd1-N2-C28	-71.22	C8-C13-C16-C21	-2.58
Cl2-Pd1-N1-C5	66.85	C12-C13-C16-C17	-3.23
Cl2-Pd1-N2-C24	-72.48	C21-C20-C24-N2	-1.32
C3-C4-C8-C9	1.42	C19-C20-C24-C25	1.47